A&A 522, A110 (2010)
DOI: 10.1051/0004-6361/201015154

Astronomy & Astrophysics

Transiting exoplanets from the CoRoT space mission⋆

XIII. CoRoT-13b: a dense hot Jupiter in transit around a star with solar metallicity and super-solar lithium content

J. Cabrera[1,2], H. Bruntt[3], M. Ollivier[4], R. F. Díaz[5], Sz. Csizmadia[1], S. Aigrain[6], R. Alonso[7], J.-M. Almenara[8], M. Auvergne[3], A. Baglin[3], P. Barge[9], A. S. Bonomo[9], P. Bordé[4], F. Bouchy[10,5], L. Carone[11], S. Carpano[12], M. Deleuil[9], H. J. Deeg[8], R. Dvorak[13], A. Erikson[1], S. Ferraz-Mello[14], M. Fridlund[12], D. Gandolfi[15,12], J.-C. Gazzano[9,16], M. Gillon[7,17], E. W. Guenther[15], T. Guillot[16], A. Hatzes[15], M. Havel[16], G. Hébrard[5], L. Jorda[9], A. Léger[4], A. Llebaria[9], H. Lammer[18], C. Lovis[7], T. Mazeh[19], C. Moutou[9], A. Ofir[19], P. von Paris[1], M. Pätzold[11], D. Queloz[7], H. Rauer[1,20], D. Rouan[3], A. Santerne[9], J. Schneider[2], B. Tingley[8], R. Titz-Weider[1], and G. Wuchterl[15]

(Affiliations can be found after the references)

Received 4 June 2010 / Accepted 28 July 2010

ABSTRACT

We announce the discovery of the transiting planet CoRoT-13b. Ground-based follow-up in CFHT and IAC80 confirmed CoRoT's observations. The mass of the planet was measured with the HARPS spectrograph and the properties of the host star were obtained analyzing HIRES spectra from the Keck telescope. It is a hot Jupiter-like planet with an orbital period of 4.04 days, 1.3 Jupiter masses, 0.9 Jupiter radii, and a density of 2.34 g cm^{-3}. It orbits a G0V star with $T_{\rm eff}$ = 5 945 K, M_* = 1.09 $M_\odot$, R_* = 1.01 $R_\odot$, solar metallicity, a lithium content of +1.45 dex, and an estimated age of between 0.12 and 3.15 Gyr. The lithium abundance of the star is consistent with its effective temperature, activity level, and age range derived from the stellar analysis. The density of the planet is extreme for its mass, implies that heavy elements are present with a mass of between about 140 and 300 $M_\oplus$.

Key words. planetary systems – techniques: photometric – techniques: radial velocities – techniques: spectroscopic

1. Introduction

Transiting planets are fundamental objects to our understanding of planetary formation and evolution. Their particular geometrical orientation allows the simultaneous measurement of their mass and radius, permitting a first order study of their internal structure. Moreover, through the careful analysis of their passages in front of (primary transit) and behind (occultation of the planet or secondary transit) their host star, a characterization of the composition and the temperature structure of their atmosphere can be carried out.

CoRoT is a space telescope dedicated to the study of asteroseismology and the discovery of extrasolar planets by the method of transits (Baglin et al. 2006). The *CoRoT* survey has previously detected, among other planets, the faint signal of a small rocky planet (CoRoT-7b; Léger et al. 2009; Queloz et al. 2009; Bruntt et al. 2010b) and a giant planet with a temperate surface temperature (CoRoT-9b; Deeg et al. 2010).

This paper presents the discovery of the planet CoRoT-13b, a dense giant planet in a close orbit around a main sequence star. Section 2 describes the observations performed with the satellite. Ground-based observations including spectroscopic characterization of the star and radial velocity measurements are reported in Sect. 3. The derivation of the planetary parameters is described in Sect. 4. A discussion of the results is presented in Sect. 5.

2. CoRoT observations

The observations of the *CoRoT* field LRa02 started on 16 November 2008; the first transits of CoRoT-13b were discovered by the Alarm Mode and the target was oversampled (the standard 512 s sampling rate was changed to 32 s; see Surace et al. 2008) between 9 December 2008 and the end of the observations in 11 March 2009, gathering in total about 250 000 photometric measurements.

The coordinates, identification labels, and magnitudes of CoRoT-13 are given in Table 1. It is a relatively faint object for *CoRoT* (V = 15.039) and it was therefore assigned a monochromatic aperture mask (for a complete description of the observing

⋆ The CoRoT space mission, launched on December 27th 2006, has been developed and is operated by CNES, with the contribution of Austria, Belgium, Brazil, ESA (RSSD and Science Programme), Germany and Spain. Part of the observations were obtained at the Canada-France-Hawaii Telescope (CFHT) which is operated by the National Research Council of Canada, the Institut National des Sciences de l'Univers of the Centre National de la Recherche Scientifique of France, and the University of Hawaii. Based on observations made with HARPS spectrograph on the 3.6-m European Organisation for Astronomical Research in the Southern Hemisphere telescope at La Silla Observatory, Chile (ESO program 184.C-0639). Based on observations made with the IAC80 telescope operated on the island of Tenerife by the Instituto de Astrofísica de Canarias in the Spanish Observatorio del Teide. Part of the data presented herein were obtained at the W. M. Keck Observatory, which is operated as a scientific partnership among the California Institute of Technology, the University of California and the National Aeronautics and Space Administration. The Observatory was made possible by the generous financial support of the W. M. Keck Foundation.

Table 1. IDs, coordinates, and magnitudes of CoRoT-13.

CoRoT window ID	LRa02_E2_2165
CoRoT ID	110839339
UCAC3	170-048045
USNO-A2 ID	0825-03324928
USNO-B1 ID	0849-0108714
2MASS ID	06505307-0505112
Coordinates	
RA (J2000)	$6^h50^m53.07^s$
Dec (J2000)	$-5°5'11.26''$
Magnitudes	

Filter	Mag	Error
B^a	15.777	0.077
V^a	15.039	0.041
r'^a	14.738	0.027
i'^a	14.304	0.033
J^b	13.710	0.021
H^b	13.406	0.027
K^b	13.376	0.038

Notes. [(a)] Provided by ExoDat (Deleuil et al. 2009); [(b)] from 2MASS catalog.

modes of the satellite, please refer to Boisnard & Auvergne 2006; Barge et al. 2008; Auvergne et al. 2009). Figure 1 shows the raw light curve (LC) of the target. One of the most significant environmental effects in *CoRoT* LCs are hot pixels, which are proton impacts that produce permanent damage to the CCD lattice (see Drummond et al. 2008; Pinheiro da Silva et al. 2008). On average, 0.3% of the pixels are affected by one of these events with an impact of more than 1000 electrons in flux during a long run (Auvergne et al. 2009). The mask of CoRoT-13b has only 69 pixels, but unfortunately this particular LC shows at least 3 impacts over the 1000-electron threshold plus some other impacts of lesser importance. These impacts do not significantly affect the characterization of the target as long as the regions affected are properly treated (Pinheiro da Silva et al. 2008).

3. Ground-based observations

3.1. Photometric measurements

A complete description of the photometric follow-up of *CoRoT* targets is given in Deeg et al. (2009). For the particular case of CoRoT-13b, photometric measurements of the host star were carried out at the 3.6 m Canada-France-Hawaii-Telescope (CFHT) in late November 2009 confirming that the transit was on-target, although with a depth slightly greater than expected because of the contribution of contaminants to the flux in the *CoRoT* mask. Later on, in early January 2010, new on-off observations were carried out at the IAC80 telescope, in Tenerife, confirming the previous results.

Figure 2 shows the region of the sky around the target taken with the Wide Field Camera of the Isaac Newton Telescope (INT/WFC) in Roque de los Muchachos. The closest contaminants to the main target, according to the ExoDat database (Deleuil et al. 2009), are shown in Table 2. In particular, the object 110839426 is included completely in the *CoRoT* mask, diluting the transit signal of CoRoT-13b. An analysis of the point spread function (PSF) of *CoRoT* reveals that the main target, the planet-hosting star, is responsible for 89 ± 1% of the flux within the mask.

3.2. Spectroscopic measurements

The star was observed with HIRES at the Keck on 5 December 2009 as part of NASA's key science programme in support of the *CoRoT* mission. We obtained one spectrum without the iodine cell and with an exposure time of 1200 s. The spectral resolution is ~45 000. To determine the atmospheric parameters of CoRoT-13, we analysed the spectrum using the VWA software (Bruntt et al. 2004, 2010a). We selected lines in the range 5050–7810 Å. A small section of the spectrum is shown in Fig. 3, where the typical signal-to-noise ratio (SNR) is 55. To determine the atmospheric parameters we used the neutral and ionized Fe lines and also the wide Ca lines at 6122 and 6162 Å (see Bruntt et al. 2010a, for a description). From this analysis we determined the parameters $T_{\rm eff} = 5\,945 \pm 90$ K, $\log g = 4.30 \pm 0.10$, [M/H] = +0.01 ± 0.07 (mean of Si, Fe and Ni), and projected rotational velocity $v \sin i = 4 \pm 1$ km s^{-1}. The $T_{\rm eff}$ was adjusted by −40 K based on the comparison of 10 stars with $T_{\rm eff}$ determined from both interferometric and spectroscopic methods as described by Bruntt et al. (2010a). The abundances of 10 elements are given in Table 3 and shown in Fig. 4. The horizontal yellow bar is the mean metallicity. Although the metallicity of this star is essentially solar, the abundance of Li I is +1.45 dex, similar to the case of another planet hosting star, CoRoT-6 (Fridlund et al. 2010).

The mass, radius, and age of the star are calculated using the Starevol evolutionary tracks (Siess 2006, Palacios, private communication). The input values are the spectroscopic parameters derived above ($T_{\rm eff}$ and [Fe/H]) and the proxy for the stellar density ($M_\star^{1/3}/R_\star$) obtained from the modeling of the transit light-curve. The results are $M_* = 1.09 \pm 0.02\ M_\odot$ and $R_* = 1.01 \pm 0.03\ R_\odot$, which gives a corresponding surface gravity of $\log g = 4.46 \pm 0.05$ in perfect agreement with the spectroscopic value. We obtain an interval for the star's age of between 0.12 and 3.15 Gyr.

Finally, using simultaneously the seven $BVr'i'JHK$s broadband magnitudes reported in Table 1 and following the method described in Gandolfi et al. (2008), we derived an interstellar extinction $A_V = 0.20 \pm 0.10$ mag and a distance to the star $d = 1060 \pm 100$ pc. Consistent results were obtained using the absolute magnitude (Allen 1973) and the intrinsic near-infrared colours (González Hernández & Bonifacio 2009) tabulated for a G0 V type star.

3.3. Radial velocity measurements

Precise radial velocity measurements of CoRoT-13 were obtained with the HARPS spectrograph between the nights of 22 November 2009 and 15 February 2010 (ESO program 184.C-0639). HARPS is a cross-dispersed echelle spectrograph fiber-fed from the Cassegrain focus of the 3.6 m telescope at La Silla Observatory, Chile (Mayor et al. 2003). Fifteen spectra with a spectral resolution $R \approx 115\,000$ were obtained using exposure times of 3600 s, and setting one of the two available fibers on the sky to monitor the presence of moonlight and help achieve optimal sky background subtraction, which is important for faint targets such as this. The SNRs per pixel of these observations at 5500 Å range from 7.1 to 11.7. Our Th-Ar calibrations exposures were adquired at the beginning of each night, which has been shown to be enough to obtain the required precision due to the high stability of the instrument.

The spectra were reduced and extracted using the HARPS pipeline, and the radial velocity was measured on each extracted spectrum by means of a weighted cross-correlation

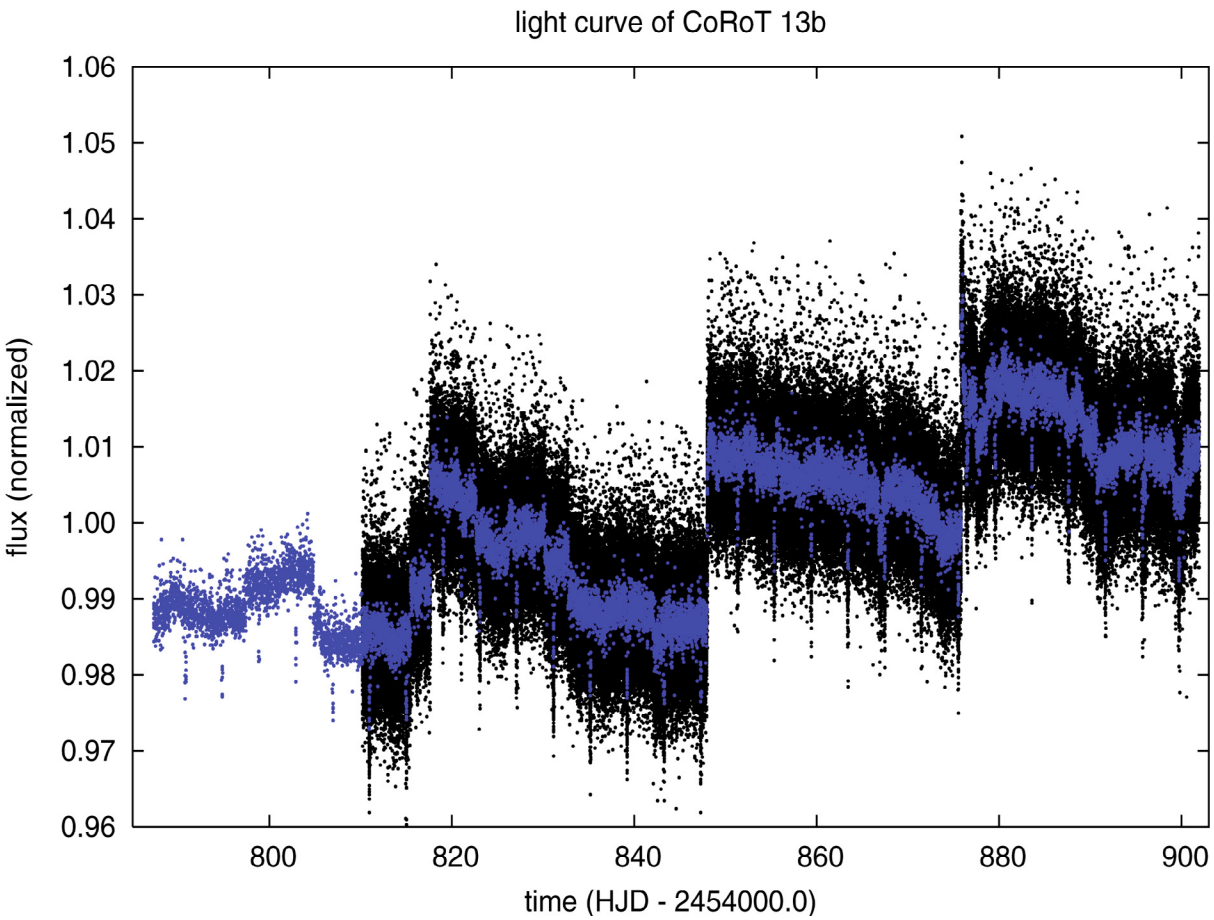

Fig. 1. Raw light curve of CoRoT-13b. The target was oversampled from 9 December 2008 (HJD 2 454 810.20); for visualization purposes, we superimpose the LC binned at a sampling rate of 512 s to the 32 s sampled region. The jumps in the data are caused by hot pixels as described in the text.

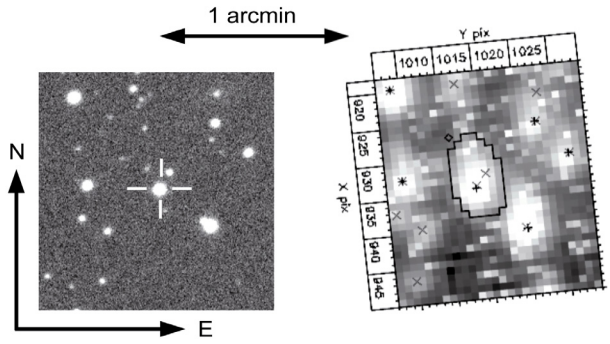

Fig. 2. Region of the sky around CoRoT-13. *Left*: image taken with INT/WFC with a resolution of 0.3″. The position of the target is indicated with a white cross. *Right*: image taken by CoRoT with the same scale and orientation; the resolution is around 2.32″/pixel. The area inside the black line is the mask used to compute the photometry; the position of the nearest contaminants from the ExoDat database are indicated with different types of crosses.

Table 2. Closest contaminants to CoRoT-13b with their respective magnitudes and relative distances to the target.

CoRoT ID	distance (arc sec)	*B*	*V*	*R*
110839426	6.58	19.354	18.136	17.625
110839769	20.14	15.424	14.689	14.395
110838938	21.58	19.691	18.412	17.838
110838780	22.79	16.927	16.066	15.701
110838726	28.34	19.911	18.489	17.875
110839832	28.44	17.611	16.749	16.388

(see Baranne et al. 1996) with a numerical mask corresponding to a G2 star. The resulting cross-correlation functions (CCFs) were fitted by Gaussians to derive the radial velocities. The measured values are listed in Table 4 and shown in Fig. 5, together with the best-fit orbital solution (see below). During some of the observations, the star fiber was contaminated by moonlight. In those cases, if the peak of the CCF produced by moonlight was expected to be close to the measured speed of the target, a correction was applied using data from the fiber recording the sky (see Bonomo et al. 2010, in preparation). Those points are shown as white circles in Fig. 5 and we added 30 m s^{-1} quadratically to the uncertainty estimated from the CCF to account for possible systematic errors introduced by the moonlight correction.

The orbital solution was found by χ^2 minimization, with the period and epoch of inferior conjunction (when radial velocity is zero after removal of the systemic velocity) being fixed to the values provided by the *CoRoT* ephemeris (which are calculated by fitting a linear regression to the centre position of the individual transits). The eccentricity of the orbit was a free parameter at first, but since the best-fit solution was compatible with a circular orbit at the two-σ level (the three-σ upper limit to the eccentricity is 0.145), we decided to fix it to $e = 0$ when determining the remaining parameters and their uncertainties. Figure 5

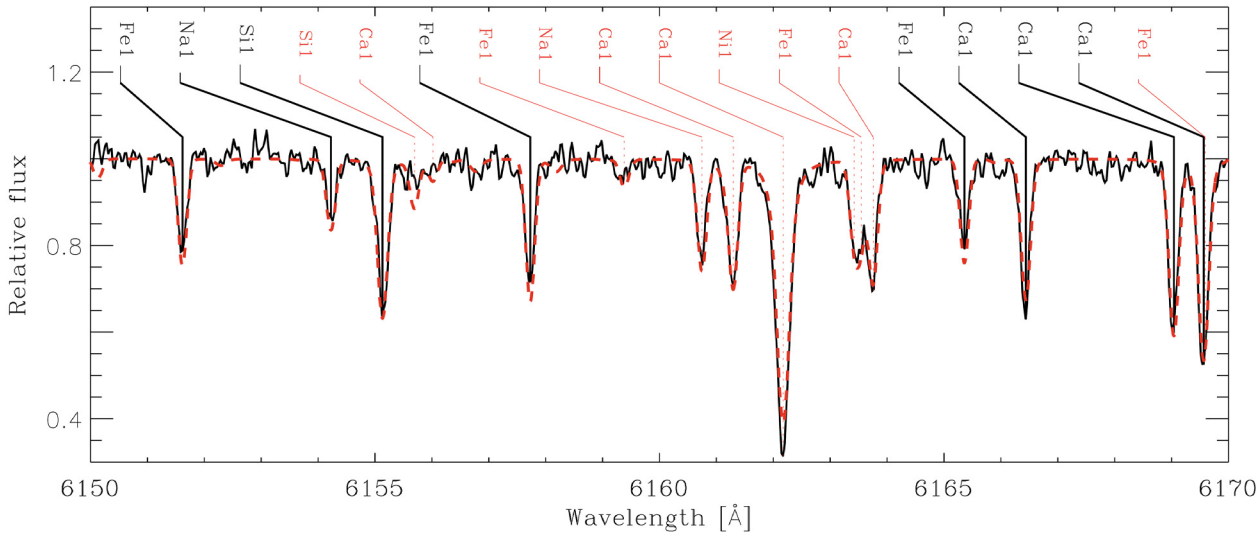

Fig. 3. Detail of the Keck spectrum of CoRoT-13 around the pressure-sensitive Ca II line at 6162 Å. The synthetic spectrum is shown with a dashed line. Spectral lines used in the abundance analysis are marked with solid vertical lines, while the other spectral lines are marked with dotted lines.

Table 3. Abundances of 10 elements in CoRoT-13 relative to the Sun.

El.	Abund.	N	El.	Abund.	N
Li I	+1.45	1	Ti I	−0.06	2
O I	+0.02	2	Ti II	+0.05 ± 0.04	2
Na I	−0.07	2	Cr I	−0.03 ± 0.16	4
Mg I	−0.07	1	Fe I	+0.03 ± 0.04	103
Si I	+0.04 ± 0.04	13	Fe II	+0.04 ± 0.05	11
Ca I	+0.03 ± 0.05	6	Ni I	−0.04 ± 0.05	25

Notes. The element name, abundance relative to the Sun, and the number of spectral lines used are given.

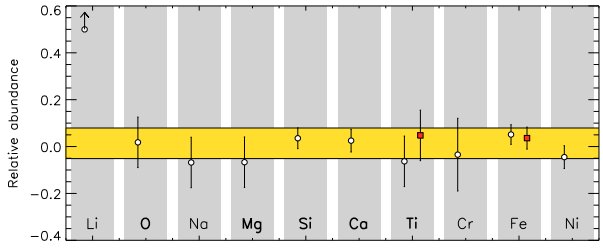

Fig. 4. Mean abundances of 10 elements in CoRoT-13 Keck spectrum. White circles correspond to neutral lines and red boxes represent singly ionized lines. The yellow area represents the mean metallicity within one σ error bar.

shows the RV measurements, phased to the *CoRoT* period, together with the best-fit circular model and the residuals; the obtained parameters are listed in Table 6. The resulting value of χ^2 is 8.2 for 13 degrees of freedom, and the rms of the residuals is 20.2 m s^{-1}, which is compatible with expectations based on the median of the RV uncertainties, 21.2 m s^{-1}. These suggest that the circular model – with the obtained parameters – adequately describes the available data.

With fixed ephemeris and eccentricity set to zero, the fitting problem is reduced to a linear least squares minimization with two free parameters. The uncertainties reported in Table 6 are therefore estimated using the covariance matrix, which has a covariance term of 6.48 m^2 s^{-2}. However, stellar activity and other long-term phenomena can produce correlated noise in the observations and hence render the above estimation of the

Table 4. Radial velocities measurements and bisector span velocities measured with HARPS.

BJD −2 455 000	RV [km s^{-1}]	σ_{RV} [km s^{-1}]	Bis [km s^{-1}]	Moon correction^a [km s^{-1}]
158.7187	22.293	0.029	0.027	
160.725	22.598	0.026	0.038	
161.7209	22.522	0.053	0.144	0.101
163.8279	22.379	0.044	−0.019	0.055
166.7245	22.311	0.037	−0.091	0.219
168.7634	22.641	0.042	−0.012	0.503
219.7315	22.296	0.02	0.036	
220.7327	22.464	0.022	−0.014	
225.6511	22.606	0.021	−0.01	
226.7338	22.45	0.021	0.059	
228.6545	22.452	0.021	−0	
237.5841	22.624	0.02	0.006	
238.5617	22.478	0.018	−0.014	
239.7142	22.304	0.019	0.024	
243.6139	22.311	0.016	−0.003	

Notes. $^{(a)}$ Difference between moonlight-corrected and uncorrected radial velocities.

uncertainties invalid. To explore this, we used the Prayer Bead method (see, for example, Désert et al. 2009; Winn et al. 2009), i.e., we performed a cyclic permutation of the residuals of the best-fit curve and fit the model again. We repeated this for every possible shift and measured the standard deviation of the obtained parameters. We also performed a similar analysis but after randomly re-ordering the residuals rather than shifting them. In this way, we constructed 10 000 synthetic data sets that were again used to fit our model. In both cases, the obtained dispersion in the parameters was found to be smaller than the error bars reported in Table 6.

The bisector analysis for these data is shown in Fig. 6, where the uncertainty in the bisector span velocity has been set to twice that of the corresponding radial velocity. The bisector span velocities do not show any clear dependence with radial velocity values and the Pearson correlation coefficient between these two magnitudes is around 0.15, which is a sign of a lack of correlation. This clearly indicates that the measured RV variations do not originate from changes in the shape in the CCF as would be

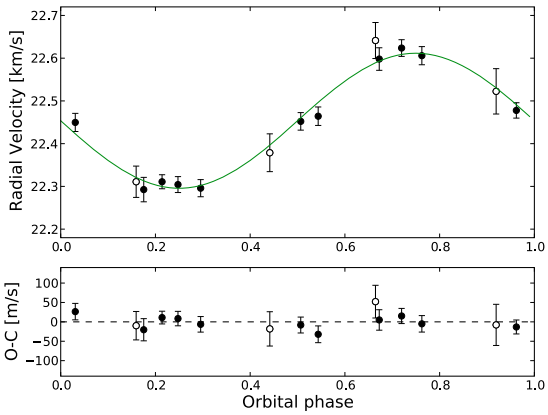

Fig. 5. *Upper panel*: radial Velocity measurements phased to the orbital period measured by *CoRoT*. The solid curve represents the best-fit solution. *Lower panel*: residuals to the fit. In both panels, the white symbols indicate the measurements that have been corrected for moonlight contamination.

the case if the system consisted of a background eclipsing binary whose light were diluted by the *CoRoT* main target. In addition, no significant changes in the measured RVs are observed when different stellar masks are used for the correlation, which more conclusively excludes the background eclipsing binary scenario.

4. Planetary parameters

The transit parameters were determined in the same manner as described in the case of CoRoT-6b (Fridlund et al. 2010). The pre-processed light curve was divided by its median, and a new light curve was constructed by convolving it with a fourth order Savitzky-Golay filter (Press et al. 2002). The standard deviation of the differences between the measured and the convolved light curves was calculated and a 5σ clip applied to remove spurious outliers. This clipping was iterated until no more outliers were found. After these steps, the light curve was folded and a bin average applied forming 5000 bins.

We used the Mandel & Agol (2002) model to perform the fit to the final, phase-folded light curve. We assumed a circular orbit and an absolutely dark planet at the CoRoT wavelength.

The six adjusted parameters were the ratios a/R_s, $k = R_{pl}/R_s$, the impact parameter $b = a\cos i/R_s$ (i is the inclination of the orbit), the two limb-darkening coefficients u_+, u_-, and the contaminant factor, which was varied across the range 10–12% (corresponding to the measured value of 11 ± 1%) to enable a more accurate estimation of errors. The quadratic limb darkening law is $I(\mu)/I(1) = 1-\mu+u_a\mu+u_b(1-\mu)^2$, and we fitted the coefficients $u_+ = u_a + u_b$ and $u_- = u_a - u_b$. The best-fit relation was found by the Harmony Search algorithm (Geem et al. 2001), a genetic-type algorithm. The 1σ errors were obtained from the width of the parameter distribution to be between χ^2_{min} and $\chi^2_{min} + 1$.

We calculated different solutions for the light curve of CoRoT-13b using different approaches to the treatment of the limb darkening parameters to understand the constraints that this effect places on the determination of the final values. The results are presented in Table 5. In model A, we allowed both u_+ and u_- to be free parameters. In models B, C, and D we fixed u_+ to be 0.81 (the value that we found in model A), 0.88 (i.e. 0.81 + 1σ) and 0.74 (0.81−1σ; where σ means the error bar of the coefficient found in model A), respectively. In model E, we fixed the limb darkening to the predicted values for the star (Sing 2010). The corresponding χ^2-values of these solutions did not differ too much from each other, showing that limb darkening is a second order effect in the transit shape. The different assumptions about the limb-darkening yielded quite consistent light curve solutions: the a/R_s, k ratios are in good agreement within their error bars for these five models. When we fixed u_+, the uncertainties in the impact parameter increased by a factor of two, despite the error bars in the impact parameters found in the B, C, D, and E solutions are overlapping with the one found in model A. The precise determination of the impact parameter is more complicated when the transit is nearly central. We learned from this experiment that fitting both limb darkening coefficients (or, what we actually did, fitting both of their combinations) yielded more precise values.

Since $u_+ = 0.81 \pm 0.07$ (Sing 2010 gives 0.662 ± 0.022 for this temperature, $\log g$, and metallicity) and $u_- = -0.09 \pm 0.09$ (Sing 2010 gives 0.156 ± 0.022) the agreement between theoretical predictions and measurements is withing 2σ error bars, which is satisfactory. We accept solution A as the definitive one (the fit is shown in Fig. 7).

5. Discussion

5.1. Stellar properties

The spectroscopic analysis of CoRoT-13 reveals a G0V star with an age of between 0.12 and 3.15 Gyr, solar metallicity ([M/H] = +0.01 ± 0.07), a high relative abundance of lithium (+1.45 dex), and a low activity level according to the analysis of activity indicators such as the H-K Ca II lines (where no emission is detected).

The rate of lithium depletion of solar-like stars is related to both the age of the star and to the depth of the convective zone, as it is destroyed at a temperature of approximately $\sim 2.5 \times 10^6$ K in the radiative region of a star (Chaboyer 1998). Given the spectral type of CoRoT-13, we expect a lower lithium depletion rate than in solar analogs (Castro et al. 2009). Using the value of the Li I abundance, we computed a $\log n(Li) = 2.55$. From Fig. 7 of Sestito & Randich (2005) and with the value of the effective temperature ($T_{eff} = 5945 \pm 90$ K), we estimated the age of the star to be in the range 300 Myr to 1 Gyr, consistent with the range from the evolutionary models. Israelian et al. (2009) claimed a lithium depletion in solar-like stars with orbiting planets, although it is not clear that previous observations support this conclusion (Meléndez et al. 2009b). CoRoT-13 is not depleted in lithium, albeit we emphasize that the effective temperature of this star is slightly higher than the upper limit for depletion given in Israelian et al. (2009).

The $v \sin i$ value indicates a rotational period of the star of around 13 days[1]. Gyrochronology (Barnes 2007) was able to be used as an age estimator. Using the improved gyrochronology relations from Mamajek & Hillenbrand (2008), we derived a gyrochronologic age of 1.66 Gyr well within the range of age given by evolutionary models. Emission lines are detected neither at the bottom of the Ca II H and K lines nor in the H_α line implying that the star belongs to the inactive population with $\log R'_H K < -5.0$. We were thus unable to derive any chromospheric age for the star. Other G0V stars are found with similar rotation rates and low activity levels (Noyes et al. 1984).

We searched for signs of stellar rotation in the light curve (LC) observed by *CoRoT* to compare with the clear signs of

[1] A lower limit, as the value of sin i for the spin axis of the star is unknown.

Table 5. Values of the adjusted parameters in the modeling of the transit of CoRoT-13b in the different approximations described in the text.

Parameter	A	B	C	D	E
a/R_*	10.81 ± 0.32	11.22 ± 0.42	11.15 ± 0.40	10.98 ± 0.48	10.89 ± 0.40
$k = R_p/R_*$	0.0909 ± 0.0014	0.0900 ± 0.0016	0.0896 ± 0.0014	0.0912 ± 0.0012	0.0914 ± 0.0011
$b = a \cos i/R_*$	0.374 ± 0.054	0.264 ± 0.097	0.271 ± 0.092	0.349 ± 0.091	0.385 ± 0.070
inclination (deg)	$88.01^{+0.35}_{-0.33}$	$88.65^{+0.57}_{-0.53}$	$88.61^{+0.54}_{-0.50}$	$88.01^{+0.58}_{-0.53}$	$87.97^{+0.43}_{-0.46}$
u_+	0.81 ± 0.07	0.81 (fixed)	0.88 (fixed)	0.74 (fixed)	0.662 (fixed)
u_-	−0.09 ± 0.09	−0.09 (fixed)	−0.24 ± 0.32	−0.01 ± 0.25	0.156 (fixed)
third light	0.11 ± 0.01	0.11 ± 0.01	0.11 ± 0.01	0.11 ± 0.01	0.11 ± 0.01
$\chi^{2(a)}$	1.00000	1.00039	0.99945	1.00077	1.00130

Notes. [(a)] Normalized to the value of solution A.

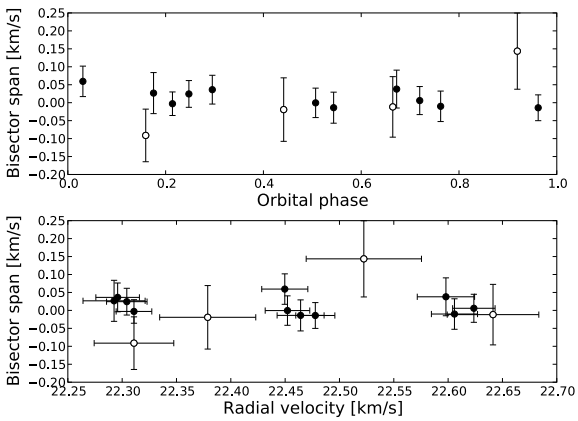

Fig. 6. Bisector analysis of the HARPS data. The white symbols represent measurements that have been corrected for moonlight contamination.

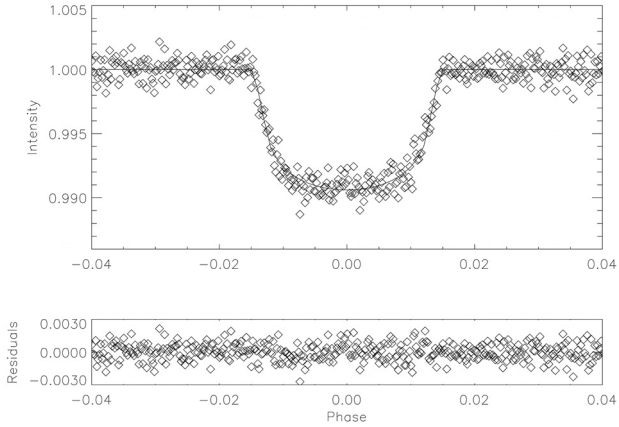

Fig. 7. Folded transit of CoRoT-13b, best-fit and its residuals using the values of solution A in Table 5.

spot modulation found in the cases of CoRoT-2b (Lanza et al. 2009b), CoRoT-4b (Lanza et al. 2009a), CoRoT-6b (Fridlund et al. 2010) or CoRoT-7b (Lanza et al. 2010). The Lomb-Scargle periodogram of the LC, once the planetary transits have been removed and the hot-pixel events treated, indeed exhibits a significant broad peak around 77 days, but no significant peak at the expected rotational frequencies. The 77 day period is comparable with the length of the run (115 days), so we may have observed an irregular pattern that, in the observing window of 115 days, has a typical timescale of variation of 77 days that may mimic an harmonic oscillation. The only reliable information about this particular signal is its characteristic amplitude of 0.5% and its characteristic timescale of 77 days; one has to be extremely cautious when interpreting its nature. Two immediate possibilities are stellar activity and an instrumental residual signal. In the latter case, straylight or other instrumental effects such as temperature fluctuations should affect a region of the CCD (if not all), instead of a single target. None of the targets in the neighborhood of CoRoT-13 show a similar pattern. Other environmental features (such as hot pixels), although present, have a completely different behaviour in terms of both amplitude and timescale and are probably not responsible for the signal. The spectroscopic analysis shows that CoRoT-13 is a quiet dwarf star. A G0V star might show spot modulation with a characteristic timescale similar to the rotational period of the star as well as long-term variations in timescales of several years (Baliunas et al. 1995), but not in the timescales considered here. On the other hand, slowly rotating giant stars might show a pattern of variability with similar amplitudes and characteristic timescales as those revealed by the periodogram. We therefore conclude that the modulation measured in the LC of CoRoT-13 is due to a background contaminant and not the main target.

Lanza (2010) found a relation between the presence of giant planets and the angular momentum loss of their host stars, such that giant planet hosting stars with $T_{\rm eff} \gtrsim 6000$ K tend to have an $n/\Omega \approx 1, 2$ orbital period/rotational period synchronization with their respective planets. The effective temperature of CoRoT-13 is immediately below this lower limit and the rotational period obtained from the spectroscopic analysis (around 13 days) is indeed longer than the expected 2:1 resonance or the synchronization. However, the rotational period is not sufficiently well constrained (the relative uncertainty is around 35%) and the inclination of the spin-axis of the star is not known. A study of the Rossiter-McLaughlin effect of this planet would infer the relative angle of inclination of the planet and the star, which is an important parameter in the model proposed by Lanza (2010).

5.2. Planet interior

Figure 8 compares CoRoT-13b to other transiting exoplanets in a mass-radius diagram. Although it is not the densest object known so far (both super-Earths and brown dwarfs may be denser), it is clearly extremely dense for its mass. This is confirmed by a combined modeling of the star and planet evolution (see Guillot & Morel 1995; Morel & Lebreton 2008; Bordé et al. 2010) shown in Fig. 9. The small planetary radius derived from the transit photometry and spectroscopy is consistent with a truly considerable amount of heavy elements in the planet. When fitting the stellar effective temperature and density within their 1σ error bars (see Table 6 and red area in Fig. 9), between about 140 and 300 $M_\oplus$ of heavy elements are required to reproduce the measured planetary size. When fitting the stellar parameters

Table 6. Planet and star parameters.

Ephemeris	
Planet orbital period P [days]	4.035 190 ± 0.000 030
Primary transit epoch $T_{\rm tr}$ [HJD-2 450 000]	4 790.809 1 ± 0.000 6
Primary transit duration $d_{\rm tr}$ [h]	3.14 ± 0.01
Results from radial velocity observations	
Orbital eccentricity e	0 (fixed)
Radial velocity semi-amplitude K [m s^{-1}]	157.8 ± 7.7
Systemic velocity $V_{\rm r}$ [km s^{-1}]	22.4536 ± 0.0060
O-C residuals [m s^{-1}]	20.2
Fitted transit parameters	
Scaled semi-major axis a/R_*	10.81 ± 0.32
Radius ratio $k = R_{\rm p}/R_*$	0.090 9 ± 0.001 4
Quadratic limb darkening coefficients[a] u_+	0.81 ± 0.07
u_-	−0.09 ± 0.09
Impact parameter[b] b	0.374 ± 0.054
	±
Deduced transit parameters	
$M_*^{1/3}/R_*$ [solar units]	1.014 ± 0.030
Stellar density ρ_* [g cm^{-3}]	1.468 ± 0.131
Inclination i [deg]	$88.02^{+0.34}_{-0.36}$
Spectroscopic parameters	
Effective temperature $T_{\rm eff}$ [K]	5 945 ± 90
Surface gravity log g [dex]	4.30 ± 0.10
Metallicity [Fe/H] [dex]	0.01 ± 0.07
Stellar rotational velocity $v \sin i$ [km s^{-1}]	4 ± 1
Spectral type	G0V
Stellar and planetary physical parameters from combined analysis	
Star mass [$M_\odot$]	1.09 ± 0.02
Star radius [$R_\odot$]	1.01 ± 0.03
Surface gravity log g [dex]	4.46 ± 0.05
Age of the star t [Gyr]	0.12 − 3.15
Distance of the system [pc]	1 060 ± 100
interstellar extinction $A_{\rm V}$ [mag]	0.20 ± 0.10
Stellar rotation period $P_{\rm rot}$ [days]	13^{+5}_{-3}
Orbital semi-major axis a [AU]	0.0510 ± 0.0031
Planet mass $M_{\rm p}$ [$M_{\rm Jup}$][c]	1.308 ± 0.066
Planet radius $R_{\rm p}$ [$R_{\rm Jup}$][c]	0.885 ± 0.014
Planet density $\rho_{\rm p}$ [g cm^{-3}]	2.34 ± 0.23
Planet surface gravity log g [dex]	3.62 ± 0.03
Average surface temperature[d] $T_{\rm p}$ [K]	∼1700

Notes. [(a)] $I(\mu)/I(1) = 1 - \mu + u_a\mu + u_b(1-\mu)^2$, where $I(1)$ is the specific intensity at the centre of the disk and $\mu = \cos\gamma$, γ being the angle between the surface normal and the line of sight; $u_+ = u_a + u_b$ and $u_- = u_a - u_b$. [(b)] $b = \frac{a\cos i}{R_*}$. [(c)] Radius and mass of Jupiter taken as 71 492 km and 1.8992×10^{30} g, respectively (Lang 1999). [(d)] Zero albedo equilibrium temperature for an isotropic planetary emission.

only within 3σ (yellow area), at least 100 $M_\oplus$ of heavy elements is still needed. In our planetary evolutions calculations, we assumed all heavy elements to be grouped into a well-defined central core, surrounded by a solar-composition envelope, with no added sources of heat. The possibility that these heavy elements may be at least partly mixed in the envelope is not expected to change these numbers significantly (Guillot 2005; Ikoma et al. 2006; Baraffe et al. 2008).

This extremely high amount of heavy elements is surprising for several reasons. First, this is probably a record – HD149026b, a Saturn-mass planet, has been known to possess

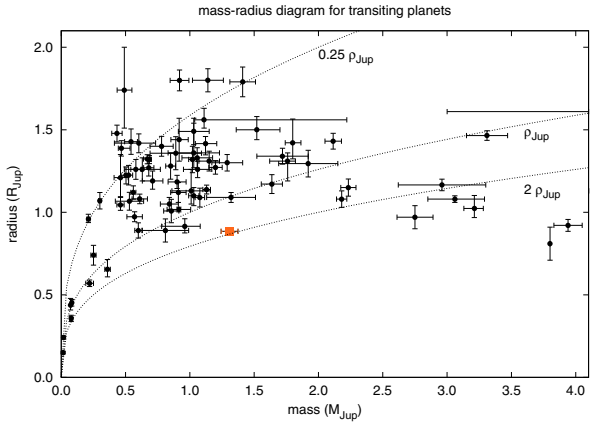

Fig. 8. Position of CoRoT-13b (square) among the other transiting planets in a mass-radius diagram.

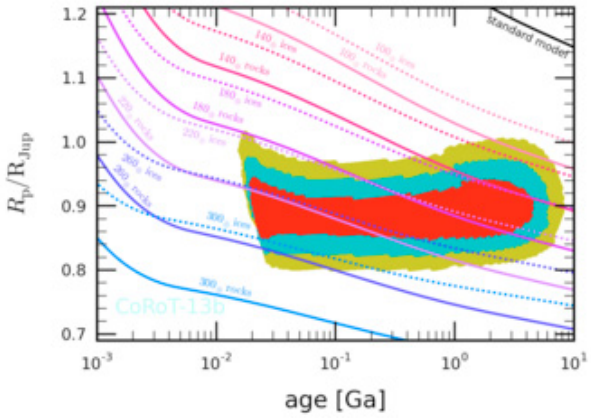

Fig. 9. Age (in Ga = 10^9 years) versus transit radius of CoRoT-13b (in Jupiter units, 1 $R_{\rm Jup}$ = 71 492 km). The coloured area correspond to constraints derived from stellar evolution models matching the stellar density and effective temperature within a certain number of standard deviation intervals of 1σ (red), 2σ (blue) or 3σ (yellow). The curves are evolution tracks for CoRoT-13b (assuming M = 1.308 $M_{\rm Jup}$, $T_{\rm eq}$ = 1700 K), with various models being labelled.

about 60–70 $M_\oplus$ of heavy elements (Sato et al. 2005; Ikoma et al. 2006). Other objects, such as OGLE-TR-56b and OGLE-TR-132b, were later found to have close to 100 $M_\oplus$ in heavy elements (Guillot et al. 2006), but no planetary-mass object has yet been shown to possess a larger amount of heavy elements. An exception may be HAT-P-2b, initially understood to have M_Z = 200 to 600 $M_\oplus$ (Baraffe et al. 2008; Leconte et al. 2009), but a revision of the stellar parameters (Torres et al. 2008) yields much smaller M_Z values for this object.

Second, planet formation models do not predict the existence of such dense objects (Mordasini et al. 2009). This is because a protoplanetary core growing beyond a few tens of Earth masses rapidly captures any surrounding hydrogen and helium, and the accretion of planetesimals is suppressed by the growth of the protoplanet beyond Saturn's mass. Giant impacts would be necessary to capture a significant mass of heavy elements (Ikoma et al. 2006).

Third, CoRoT-13b is a counterexample outside the correlation between stellar metallicity and planetary mass in heavy elements (Guillot et al. 2006; Burrows et al. 2007; Guillot 2008). One interesting possibility however is related to the high lithium abundance of the star. If the metallicity of stars with planets did provide information about the late accretion of

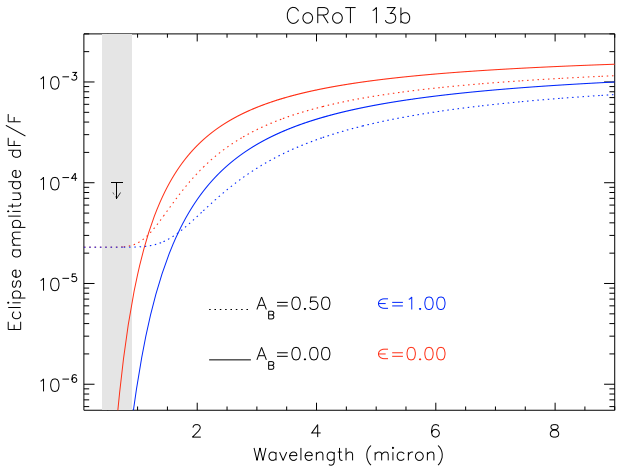

Fig. 10. Expected amplitude of the occultation of the planet as a function of the wavelength for two extreme values for the heat redistribution factor for CoRoT-13b (as defined by Cowan & Agol 2010; $\epsilon = 1$: uniform heat distribution over the planet; $\epsilon = 0$ no distribution) and two values of the Bond albedo. The gray shaded area is the wavelength window observed by *CoRoT*. The black arrow is the upper limit of *CoRoT* observations.

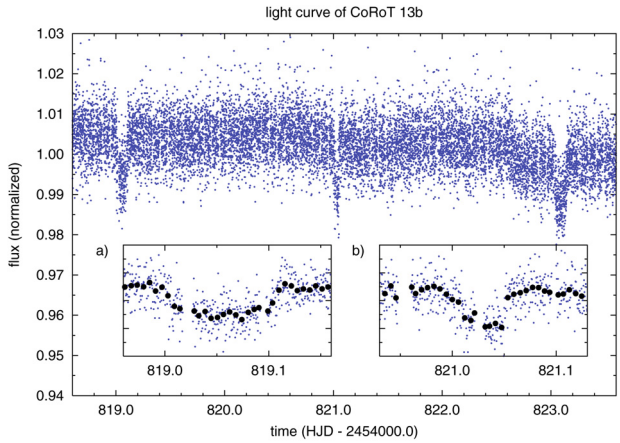

Fig. 11. Raw light curve of CoRoT-13b between the observed transits number 8 (HJD = 2 454 819.06) and 9 (HJD = 2 454 823.09) where a) describes the 8th transit and b) describes the event at HJD = 2 454 821.03, which mimics the transit of a long-period planetary companion.

circumstellar gas filtered of their heavy elements by planet formation (Meléndez et al. 2009b; Ramírez et al. 2009; Nordlund 2009), then the CoRoT-13 system may be metal-rich, even though a heavy-element poor, lithium-rich rare last burst of accretion modified the chemical properties of the star's thin outer convective zone.

5.3. Thermal losses

We estimated the thermal mass loss of CoRoT-13b by using the method and formulae described in Lammer et al. (2009), and found a negligible escape rate that did not influence the planet mass over its history. The reason for the negligible thermal mass loss of CoRoT-13b is the planet compactness and high density of about 2.34 g cm^{-3}.

5.4. Occultation of the planet by the star

In the visible wavelength range, occultations of planets behind their host stars have been detected in only a few cases: Corot-1b (Snellen et al. 2009; Alonso et al. 2009a) and CoRoT-2b (Alonso et al. 2009b; Snellen et al. 2010) in data from *CoRoT*, and HAT-P-7 in data from Kepler (Borucki et al. 2009). All of these occultations are related to inflated giant planets ($R_p > 1.4\ R_{Jup}$) on very short orbits, which means that they have large surfaces that tend to produce a large amount of reflected light and additionally are very hot ($T_{eff} > 2000$ K), which is indicative of thermal emission in the visible regime. Using the definition from Cowan & Agol (2010), CoRoT-13b, in the most favourable case (zero albedo, zero heat redistribution factor represented by the upper solid line in Fig. 10), should have an average surface temperature of around 1700 K. The emission of the planet in the visible range observed by *CoRoT* is therefore dominated by reflection, meaning that eclipse amplitudes larger than 2.5×10^{-5} cannot be expected, even with a very high Bond albedo of $A_B = 0.5$ (Fig. 10, dotted lines). This signal is not however detectable in the current data, as the measured scatter in the folded and binned light curve is on the order of 10^{-4}.

5.5. Constraints on the presence of additional planets.

The region of the light curve (LC) shown in Fig. 11, between the 8th and the 9th transits observed by *CoRoT* shows a feature that mimics a single planetary transit that is not related to the pattern of transits of CoRoT-13b. Almost in the middle of the two regular transits, we find a short feature, roughly 1.5 h long and 1% deep, which in principle could be due to a planetary transit from an additional planet in the system. This feature does not repeat in the LC, hence a hypothetical companion would require a period longer than the 80 days that remained until either end of the observations. Nevertheless, the duration of a planetary transit is linked to the period of the orbit (Seager & Mallén-Ornelas 2003) and for an 80 day orbit we expect a transit of around 8 h long. Of course, some corrections have to be done in the case the orbit is eccentric (Carter et al. 2008; Kipping 2008); but in our case, we would have to assume an eccentricity of 0.94 (and a favourable orientation) for the hypothetical planet to account for a 1.5 h long transit in this long period orbit. However, this hypothetical planet would have a periastron passage inside the orbit of CoRoT-13b. There are studies of the planetary three-body problem with high eccentricities (see for example Beaugé & Michtchenko 2003; Michtchenko et al. 2006), but to the knowledge of the authors there is no possible justification of the dynamical stability of one system formed by a close-in Jupiter-like planet in a circular orbit and a highly eccentric Jupiter-sized companion.

Moreover, there is no hint of the drift produced by any additional planet in the scatter of the residuals of the circular radial velocity (RV) analysis. The region of the parameter space of an additional planet in a circular orbit that can be discarded based on RV data is shown in Fig. 12. We note that for periods below 85 days (the span of HARPS observations), only planets in circular orbits with masses below ~0.45 M_{Jup} are not discarded by RV data. The mass limit for eccentric orbits is even lower in this range of periods, as the amplitude K of the RV movement grows as $(1 - e^2)^{-1/2}$.

Given these findings, the most simple explanation is an environmental effect that mimics a transit.

6. Summary

We have reported the discovery of CoRoT-13b, a transiting giant planet orbiting the star *CoRoT* 110839339. Our spectroscopic

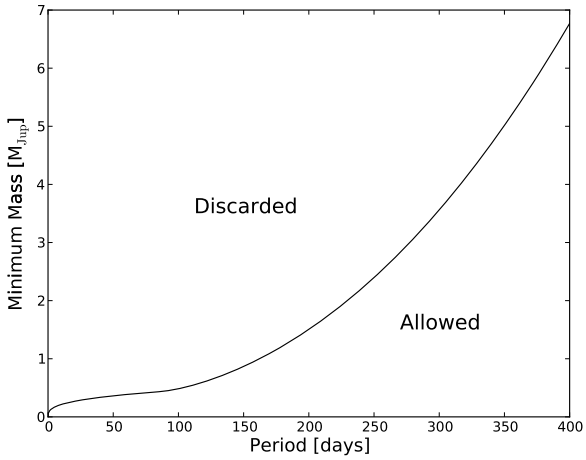

Fig. 12. Parameter space of the additional planets in the system that can been discarded on the basis of current HARPS measurements. The region above the curve is discarded by RV measurements, while planets located in the region below the curve would produce an undetectable signal.

analysis indicates that CoRoT-13 is a G0V star with $T_{\rm eff}$ = 5 945 ± 90 K, M_* = 1.09 ± 0.02 $M_\odot$, R_* = 1.01 ± 0.03 $R_\odot$, solar metallicity ([M/H] = +0.01 ± 0.07), and a high relative abundance of lithium (+1.45 dex). The evolutionary tracks constrain the age of the star to be between 0.12 and 3.15 Gyr. The results of the study of the lithium abundance, the $v \sin i$, and the activity level (which is low in both the spectroscopic and the photometric analyse) are consistent with the spectral type and the age range of the star. However, the lower limit to the interval is not favoured due to the low activity level measured.

CoRoT-13b is the highest-density jovian planet among its relatives with masses between 0.2 and 2.5 Jupiter masses. Its extreme density implies the existence of a significant amount, between 140 and 300 $M_\oplus$, of heavy elements in the planet, which contradicts the expected link between M_Z of a planet and the metalliciy of its host stars (Guillot et al. 2006; Burrows et al. 2007; Guillot 2008). There is no hint of any other massive companion in the system, which is quite a common finding for hot Jupiters.

We have discussed the consequences of this characterization and we presented evidence that this particular target provides important information about the knowledge of the interactions between the structure of stars, the formation of planets, and their joint evolution (Ikoma et al. 2006; Ammler-von Eiff et al. 2009; Meléndez et al. 2009a; Nordlund 2009; Ramírez et al. 2009; Lanza 2010).

Acknowledgements. The team at IAC acknowledges support by grant ESP2007-65480-C02-02 of the Spanish Ministerio de Ciencia e Innovación. This research has made use of the ExoDat database, operated at LAM-OAMP, Marseille, France, on behalf of the CoRoT/Exoplanet program. This publication makes use of data products from the Two Micron All Sky Survey, which is a joint project of the University of Massachusetts and the Infrared Processing and Analysis Center/California Institute of Technology, funded by the National Aeronautics and Space Administration and the National Science Foundation. This research has made use of NASA's Astrophysics Data System.

References

Allen, C. W. 1973, Astrophysical quantities (London: University of London, Athlone Press), 3rd edn.
Alonso, R., Alapini, A., Aigrain, S., et al. 2009a, A&A, 506, 353
Alonso, R., Guillot, T., Mazeh, T., et al. 2009b, A&A, 501, L23
Ammler-von Eiff, M., Santos, N. C., Sousa, S. G., et al. 2009, A&A, 507, 523
Auvergne, M., Bodin, P., Boisnard, L., et al. 2009, A&A, 506, 411
Baglin, A., Auvergne, M., Boisnard, L., et al. 2006, in COSPAR, Plenary Meeting, 36th COSPAR Scientific Assembly, 36, 3749
Baliunas, S. L., Donahue, R. A., Soon, W. H., et al. 1995, ApJ, 438, 269
Baraffe, I., Chabrier, G., & Barman, T. 2008, A&A, 482, 315
Baranne, A., Queloz, D., Mayor, M., et al. 1996, A&AS, 119, 373
Barge, P., Baglin, A., Auvergne, M., & the CoRoT team. 2008, in IAU Symp., 249, 3
Barnes, S. A. 2007, ApJ, 669, 1167
Beaugé, C., & Michtchenko, T. A. 2003, MNRAS, 341, 760
Boisnard, L., & Auvergne, M. 2006, in ESA SP 1306, ed. M. Fridlund, A. Baglin, J. Lochard, & L. Conroy, 19
Bordé, P., Bouchy, F., Deleuil, M., et al. 2010, A&A, 520, A66
Borucki, W. J., Koch, D., Jenkins, J., et al. 2009, Science, 325, 709
Bruntt, H., Bikmaev, I. F., Catala, C., et al. 2004, A&A, 425, 683
Bruntt, H., Bedding, T. R., Quirion, P., et al. 2010a, MNRAS, 405, 1907
Bruntt, H., Deleuil, M., Fridlund, M., et al. 2010b, A&A, 519, A51
Burrows, A., Hubeny, I., Budaj, J., & Hubbard, W. B. 2007, ApJ, 661, 502
Carter, J. A., Yee, J. C., Eastman, J., Gaudi, B. S., & Winn, J. N. 2008, ApJ, 689, 499
Castro, M., Vauclair, S., Richard, O., & Santos, N. C. 2009, A&A, 494, 663
Chaboyer, B. 1998, in New Eyes to See Inside the Sun and Stars, ed. F.-L. Deubner, J. Christensen-Dalsgaard, & D. Kurtz, IAU Symp., 185, 25
Cowan, N. B., & Agol, E. 2010, ApJ, submitted
Deeg, H. J., Gillon, M., Shporer, A., et al. 2009, A&A, 506, 343
Deeg, H. J., Moutou, C., Erikson, A., et al. 2010, Nature, 464, 384
Deleuil, M., Meunier, J. C., Moutou, C., et al. 2009, AJ, 138, 649
Désert, J., Lecavelier des Etangs, A., Hébrard, G., et al. 2009, ApJ, 699, 478
Drummond, R., Lapeyrere, V., Auvergne, M., et al. 2008, A&A, 487, 1209
Fridlund, M., Hébrard, G., Alonso, R., et al. 2010, A&A, 512, A14
Gandolfi, D., Alcalá, J. M., Leccia, S., et al. 2008, ApJ, 687, 1303
Geem, Z. G., Kim, J. H., & Loganathan, G. V. 2001, Simulation, 76, 60 http://sim.sagepub.com/cgi/content/abstract/76/2/60
González Hernández, J. I., & Bonifacio, P. 2009, A&A, 497, 497
Guillot, T. 2005, Ann. Rev. Earth Planetary Sci., 33, 493
Guillot, T. 2008, Phys. Scripta T, 130, 014023
Guillot, T., & Morel, P. 1995, A&AS, 109, 109
Guillot, T., Santos, N. C., Pont, F., et al. 2006, A&A, 453, L21
Ikoma, M., Guillot, T., Genda, H., Tanigawa, T., & Ida, S. 2006, ApJ, 650, 1150
Israelian, G., Delgado Mena, E., Santos, N. C., et al. 2009, Nature, 462, 189
Kipping, D. M. 2008, MNRAS, 389, 1383
Lammer, H., Odert, P., Leitzinger, M., et al. 2009, A&A, 506, 399
Lang, K. R. 1999, Astrophysical formulae, ed. K. R. Lang
Lanza, A. F. 2010, A&A, 512, A77
Lanza, A. F., Aigrain, S., Messina, S., et al. 2009a, A&A, 506, 255
Lanza, A. F., Pagano, I., Leto, G., et al. 2009b, A&A, 493, 193
Lanza, A. F., Bonomo, A. S., Moutou, C., et al. 2010, A&A, 520, A53
Leconte, J., Baraffe, I., Chabrier, G., Barman, T., & Levrard, B. 2009, A&A, 506, 385
Léger, A., Rouan, D., Schneider, J., et al. 2009, A&A, 506, 287
Mamajek, E. E., & Hillenbrand, L. A. 2008, ApJ, 687, 1264
Mandel, K., & Agol, E. 2002, ApJ, 580, L171
Mayor, M., Pepe, F., Queloz, D., et al. 2003, The Messenger, 114, 20
Meléndez, J., Asplund, M., Gustafsson, B., & Yong, D. 2009a, ApJ, 704, L66
Meléndez, J., Ramírez, I., Casagrande, L., et al. 2009b, Ap&SS, 221
Michtchenko, T. A., Beaugé, C., & Ferraz-Mello, S. 2006, Celestial Mechanics and Dynamical Astronomy, 94, 411
Mordasini, C., Alibert, Y., Benz, W., & Naef, D. 2009, A&A, 501, 1161
Morel, P., & Lebreton, Y. 2008, Ap&SS, 316, 61
Nordlund, A. 2009, ApJL, submitted
Noyes, R. W., Hartmann, L. W., Baliunas, S. L., Duncan, D. K., & Vaughan, A. H. 1984, ApJ, 279, 763
Pinheiro da Silva, L., Rolland, G., Lapeyrere, V., & Auvergne, M. 2008, MNRAS, 384, 1337
Press, W. H., Teukolsky, S. A., Vetterling, W. T., & Flannery, B. P. 2002, Numerical Recipes in C++, 2nd edn. (Cambridge University Press)
Queloz, D., Bouchy, F., Moutou, C., et al. 2009, A&A, 506, 303
Ramírez, I., Meléndez, J., & Asplund, M. 2009, A&A, 508, L17
Sato, B., Fischer, D. A., Henry, G. W., et al. 2005, ApJ, 633, 465
Seager, S., & Mallén-Ornelas, G. 2003, ApJ, 585, 1038
Sestito, P., & Randich, S. 2005, A&A, 442, 615
Siess, L. 2006, A&A, 448, 717
Sing, D. K. 2010, A&A, 510, A21
Snellen, I. A. G., de Mooij, E. J. W., & Albrecht, S. 2009, Nature, 459, 543
Snellen, I. A. G., de Mooij, E. J. W., & Burrows, A. 2010, A&A, 513, A76
Surace, C., Alonso, R., Barge, P., et al. 2008, in Presented at the Society of Photo-Optical Instrumentation Engineers (SPIE) Conference, SPIE Conf. Ser., 7019
Torres, G., Winn, J. N., & Holman, M. J. 2008, ApJ, 677, 1324
Winn, J. N., Holman, M. J., Henry, G. W., et al. 2009, ApJ, 693, 794

[1] Institute of Planetary Research, German Aerospace Center, Rutherfordstrasse 2, 12489 Berlin, Germany
e-mail: juan.cabrera@dlr.de
[2] LUTH, Observatoire de Paris, UMR 8102 CNRS, Université Paris Diderot, 5 place Jules Janssen, 92195 Meudon, France
[3] LESIA, UMR 8109 CNRS, Observatoire de Paris, UPMC, Université Paris-Diderot, 5 place J. Janssen, 92195 Meudon, France
[4] Institut d'Astrophysique Spatiale, Université Paris XI, 91405 Orsay, France
[5] Institut d'Astrophysique de Paris, UMR 7095 CNRS, Université Pierre & Marie Curie, 98bis boulevard Arago, 75014 Paris, France
[6] Department of Physics, Denys Wilkinson Building Keble Road, Oxford, OX1 3RH, UK
[7] Observatoire de l'Université de Genève, 51 chemin des Maillettes, 1290 Sauverny, Switzerland
[8] Instituto de Astrofísica de Canarias, 38205 La Laguna, Tenerife, Spain
[9] Laboratoire d'Astrophysique de Marseille, 38 rue Frédéric Joliot-Curie, 13388 Marseille Cedex 13, France
[10] Observatoire de Haute Provence, 04670 Saint Michel l'Observatoire, France
[11] Rheinisches Institut für Umweltforschung an der Universität zu Köln, Aachener Strasse 209, 50931, Germany
[12] Research and Scientific Support Department, ESTEC/ESA, PO Box 299, 2200 AG Noordwijk, The Netherlands
[13] University of Vienna, Institute of Astronomy, Türkenschanzstr. 17, 1180 Vienna, Austria
[14] IAG-Universidade de Sao Paulo, Brasil
[15] Thüringer Landessternwarte, Sternwarte 5, Tautenburg 5, 07778 Tautenburg, Germany
[16] Université de Nice-Sophia Antipolis, CNRS UMR 6202, Observatoire de la Côte d'Azur, BP 4229, 06304 Nice Cedex 4, France
[17] University of Liège, Allée du 6 août 17, Sart Tilman, Liège 1, Belgium
[18] Space Research Institute, Austrian Academy of Science, Schmiedlstr. 6, 8042 Graz, Austria
[19] School of Physics and Astronomy, Raymond and Beverly Sackler Faculty of Exact Sciences, Tel Aviv University, Tel Aviv, Israel
[20] Center for Astronomy and Astrophysics, TU Berlin, Hardenbergstr. 36, 10623 Berlin, Germany